IEEE Photonics Journal
An IEEE Photonics Society Publication

Optical Properties of Chromium and Erbium Co-Doped Alumina–Germania–Calcia–Yttria–Silica Based Fiber

(Invited Paper)

Volume 11, Number 6, December 2019

Alexander V. Kir'yanov
Debjit Dutta
Shyamal Das
Anirban Dhar
Mukul Chandra Paul

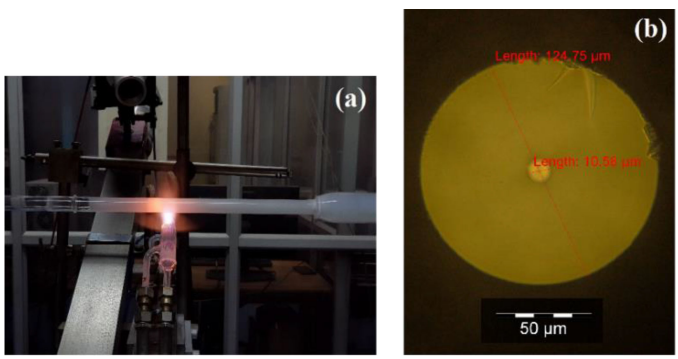

DOI: 10.1109/JPHOT.2019.2950144

Optical Properties of Chromium and Erbium Co-Doped Alumina–Germania–Calcia–Yttria–Silica Based Fiber

(Invited Paper)

Alexander V. Kir'yanov, Debjit Dutta, Shyamal Das, Anirban Dhar, and Mukul Chandra Paul

[1]Centro de Investigaciones en Optica, Leon 37150, Mexico
[2]CSIR—Central Glass and Ceramics Research Institute, Kolkata 700032, India

DOI:10.1109/JPHOT.2019.2950144

Manuscript received July 29, 2019; revised September 16, 2019; accepted October 24, 2019. Date of publication October 28, 2019; date of current version November 14, 2019. The work of D. Dutta, S. Das, A. Dhar, and M. C. Paul was supported by the Department of Science and Technology—Nano Mission, Government of India. Corresponding author: Alexander V. Kir'yanov (e-mail: kiryanov@cio.mx).

Abstract: We report the fabrication details and optical characterization of novel Erbium (Er) and Chromium (Cr) co-doped alumina-germania-calcia-yttria-silica fiber. Co-doping with Er and Cr is chosen as potentially promising for enhancing the fiber's fluorescent and amplifying potential in the near-infrared (NIR) region at 'resonant' (viz. into Er band absorption maximum, @976 nm) and 'non-resonant' (viz. off Er band while into Cr broad absorption band, @905/1064 nm) excitations. Our results reveal strong coupling, at both kinds of excitation, of Er- and Cr- subsystems in the fiber. This effect is justified by the presence of pronounced 1.5–1.6 μm emission, characteristic to Er ions, at 905/1064 nm excitations and, at 976-nm excitation, by notable spectral broadening of the fiber's NIR fluorescence and gain, comprising the lines inherent to Er^{3+} (1.5–1.6 μm) and Cr^{3+}/Cr^{4+} (1.15–1.45 μm), as compared to purely Er-doped silicate fiber, exemplified here by commercial 'L20' (Er20-4/125) and 'L40' (Er40-4/125) fibers.

Index Terms: Fiber design and fabrication, lasers, fiber, fiber optics amplifiers and oscillators.

1. Introduction

Interest to new optical silica-based fibers with pronounced fluorescence and amplifying capacity in the near-infrared (NIR) region beyond 1 μm and as broadband as possible was growing in the recent years as per a call of nowadays telecom and other (laser, medical, military etc.) applications. However, a very limited number of 'active' fibers are currently known as confirmed candidates for industrial usage for this spectral domain. In fact, a spectral gap between well-developed Ytterbium (Yb) doped fibers and Erbium doped fibers (EDFs) with operation ranges covering 1.0–1.15 μm and 1.50–1.65 μm, respectively, is still open, at least for high-power lasers/amplifiers. This unfavorable situation remains to occur despite such candidates as Bismuth (Bi) [1]–[3] and Chromium (Cr) [4], [5] doped silica fibers, which possess fluorescence bands in NIR (1.1–1.7 μm), were proposed and partly investigated during the last two decades. Each of the mentioned types of fiber has its own

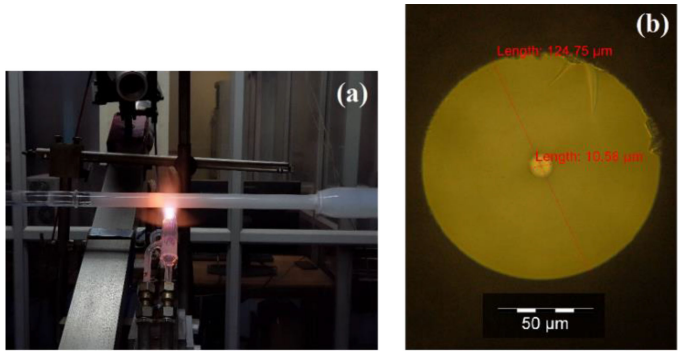

Fig. 1. (a) Snapshot of porous SiO_2-GeO_2 layer deposition onto the preform at MCVD and (b) cross-sectional view of final Cr, Er AGCYS fiber.

drawbacks, limiting their further utilization for practical needs. Among other problems note such factors as misunderstanding of the type of active centers responsible for NIR emission/amplifying and low content of active dopants, inherent to effective operation (in the case of Bi-doped fibers), and technological difficulties in attempt to stabilize a proper valence of Cr ions (usually, Cr^{3+}/Cr^{4+}) along with internal problems of room-temperature operation (in the case of Cr-doped fibers). Furthermore, an idea to co-dope silica fibers with multiple active ions attracted great deal of attention in the recent years; see e.g., [6]. Particularly, co-doping of EDFs with some other rare-earth ions such as Yb and Thulium was intensively tested in the past time. Say, such kind of co-doping as Yb/Er was found promising for high-power applications at 1.5–1.6 μm using double-clad fibers. Meanwhile, co-doping of EDFs with ions of other types was only tackled; in this sense, note a recent line of studies with such kind of co-doping as Bi/Er [7]–[12], mainly focused on attaining ultrabroad-band fluorescence and extended gain in the NIR. In turn, the Er gain broadening and spectral plaining becomes a hot task for multiwavelength generation and, eventually, for terahertz photonics; see e.g., [13]–[17] and references therein. Meanwhile, co-doping EDFs with Cr ions was, to the best of our knowledge, unknown for silica-based fibers, mostly because of the mentioned problem of stabilization of Cr ions with proper (Cr^{3+}/Cr^{4+}) valency, which is a prerequisite for their applications in the NIR (though for bulk materials this kind of co-doping was somewhat successful; see e.g., [18]). However, our recent studies in the area [19], [20] have shown certain promises that provides suitable organization of a silica-based fiber core's lattice for stabilizing Cr^{3+}/Cr^{4+} ions. As a natural continuation of that research, we present herein the details of fabrication, material characterization, and analysis of basic optical properties (including absorption, fluorescence, and gain) of Cr, Er co-doped silica-based fiber, a novel type of active optical fiber for NIR applications.

2. Fabrication and Material Properties

The fabrication of Cr, Er co-doped optical preform based on alumina-germania-calcia-yttria-silica (AGCYS) glass was done through the modified chemical vapor deposition (MCVD) process [21], [22] in combination with solution doping (SD) technique. The deposition of porous SiO_2-GeO_2 layer was performed at a high (1350 $\pm$ 10 °C) temperature into a silica tube with 20/17 mm outer/inner diameters, followed by soaking of the porous layer for subsequent incorporating at SD of different precursors (co-dopants) in suitable composition. The deposition temperature at MCVD was monitored using an IR pyrometer, moved synchronously with an oxy-hydrogen burner along the tube in forward direction. A snapshot of the deposition process is shown in Fig. 1(a). The co-dopants (Al, Er, Cr, Ca, and Y) were introduced into the porous frit employing the procedure, described in [19], [23]. The doping levels of different co-dopants inside the core were optimized through variation of the solution strength of the following precursors: $ErCl_3$: $6H_2O$, $AlCl_3$: $6H_2O$, $CrCl_3$: $6H_2O$, $CaCl_2$: $6H_2O$, and $Y(NO_3)_3$: xH_2O (all chemicals – *Alfa Aesar*), dissolved into double distilled water. The

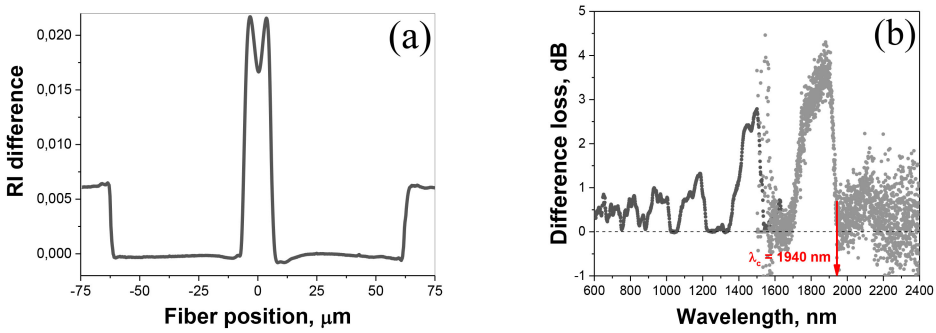

Fig. 2. (a) RI profile of Cr, Er AGCYS fiber and (b) its loss difference spectrum, measured in straight and coiled positions (arrow shows the spectral position of inferred cutoff wavelength, ~1.94 μm).

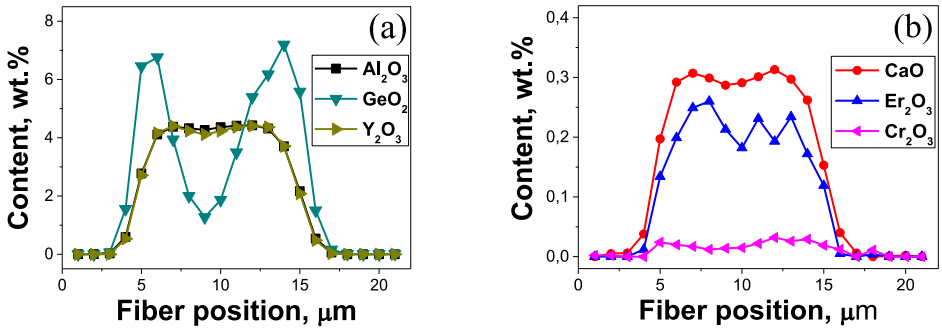

Fig. 3. Radial distributions of co-dopants (a) Al_2O_3, GeO_2, and Y_2O_3 and (b) CaO, Er_2O_3 and Cr_2O_3 in the core area of Cr, Er AGCYS fiber.

porous layer soaked for one hour was air-dried and remounted on the glass working lathe, followed by subsequent processing to obtain the final preform. The final fiber was drawn from the preform using a standard tower with on-line resin coating. The cross-sectional image of the fabricated Cr, Er AGCYS fiber, obtained using an *Olympus BX51* microscope, is shown in Fig. 1(b); its outer (cladding) and inner (core) diameters were measured to be ~125.0 and ~10.5 μm, respectively.

The refractive index (RI) profile of the Er, Cr AGCYS fiber, measured using a fiber analyzer *NR-9200 EXFO*, is presented in Fig. 2(a). Its average numerical aperture (NA) was found to be ~0.23 (in step-index approximation). The fiber's cut-off wavelength (λ_c) was obtained using a 'white-light' (WL) source with output fiber adapter (*Yokogawa AQ4305*) and a set of optical-spectrum analysers with optical bands 400–1650 nm (OSA1: *ANDO 6315A*) and 1200–2400 nm (OSA2: *Yokogawa AQ6370B*), employing standard transmission measurements with a fiber sample placed in straight and coiled positions. The result (the difference loss found from these two measurements), is shown in Fig. 2(b). As seen, given the result of the experiment, the Er, Cr AGCYS fiber guides light in slightly multimode regime in the spectral range of our main interest (1.1–1.7 μm). Regarding the cut-off wavelength found experimentally ($\lambda_c \sim 1.94\,\mu$m), it seems that it may be underestimated given that our spectral equipment is not sensitive beyond 2.4 μm. According to our theoretical estimates, a 'real' λ_c (the wavelength beyond which this fiber ought to guide only the fundamental LP_{01} mode) may be located above: indeed, if for the series of LP_{0i} modes the experimental data are believable (LP_{02} mode should be cut off at ~3.0 μm), for the series of LP_{1i} modes, the index-lowest mode LP_{11} should be cut off at around ~3.3 μm.

The elemental composition of the Er, Cr AGCYS fiber was inspected using electron probe micro-analysis (EPMA). The co-dopants' cross-sectional profiles in the fiber's core area are shown in Fig. 3; their maximum doping levels were found to be 7.1 wt.% (GeO_2), 4.3 wt.% (Al_2O_3), 4.3 wt.%

TABLE 1
Basic Parameters of Er, Cr AGCYS Fiber

Dopants concentrations (wt.%)	Core / Clad diameters (μm)	N.A.	Cutoff wavelength (μm)	Absorption (α_0) / gain (g_0) (dB/m)	Absorption contrast α^F_{NL}/α_0	Fluorescence lifetime (ms)
Er_2O_3 = 0.23 Al_2O_3 = 4.31 GeO_2 = 7.12 Y_2O_3 = 4.32 Cr_2O_3 =0.03 CaO =3.10	10.6 / 124.8	0.23	1.94 (current experiment)	32 / 28 (Er^{3+} band) 4...5 / 3...4 (Cr^{3+}/Cr^{4+} band)	0.03 (@976 nm) 0.08 (@905/1064 nm)	9.8 (Er^{3+}) 0.04 (Cr^{3+}/Cr^{4+})

(Y_2O_3), 0.025 wt.% (Cr_2O_3), 0.23 wt.% (Er_2O_3), and 3.1 wt.% (CaO). Note here that co-doping with Er and Cr was intended to get NIR emissions (beyond $\sim$1 μm: see the spectral analysis in Section 3); Al and Ge were introduced to manage RI profile of the fiber (refer to Fig. 2(a)), addition of Y was chosen to enhance fluorescent abilities of the optically active elements (Er and Cr), while that of Ca – to facilitate stabilization of Cr ions in tetrahedral (Cr^{4+}) state, mostly responsible for fluorescence beyond $\sim$1.2 μm. Also note that, according to the glass technology principles, with increasing content of a structural modifier such as Y, interstitial gap in glass network can be increased via creating of a large amount of non-bridging oxygens, which facilitates dissolving of other atoms of lattice (in our case, Cr and Er) into silica-based glass and hence diminishes their clustering.

Notice, regarding Fig. 3, that the central dip in Ge content arises due to partial escaping of gaseous GeO form during collapsing of the preform as per the following reaction [24]: $GeO_2 \leftrightarrow$ GeO (gas)$\uparrow + \frac{1}{2}O_2\uparrow$. The thermal decomposition rate for formation of gaseous GeO is very high as compared to the other elements during the collapsing stage. On the other hand, no obvious central dip in Al and Y contents happened due to high decomposition temperature of Al_2O_3, Y_2O_3, and Y_2O_3 as compared to that of GeO_2. Furthermore, as the doping levels of Cr_2O_3 and CaO are rather low, such dips are not reflected in their contents' profiles though they have lower thermal decomposition temperatures as compared to Al_2O_3, Er_2O_3 and Y_2O_3.

The basic optical characteristics of the Er, Cr AGCYS fiber are summarized in Table 1.

3. Optical Properties

3.1 Linear Absorption

The loss spectrum of the Cr, Er AGCYS fiber was measured using the cutback method. Output light from the WL source was directly launched into Cr, Er AGCYS fiber and its transmitted part was recorded with the OSAs. The measured transmission spectrum was re-calculated in the loss (absorption) spectrum, $\alpha_0(\lambda)$, shown in Fig. 4.

As seen from the figure, the spectrum demonstrates superposition of the spectral attributes of Er^{3+} ions (see the characteristic absorption peaks marked by arrows) and Cr^{3+} / Cr^{4+} ions seen as the broad absorption band with the contribution of Cr^{3+} ions prevailing at 600–1000 nm and that of Cr^{4+} ions – at longer wavelengths, beyond $\sim$1 μm. The maximum absorption within Er-band (@1530 nm) is $\sim$32 dB/m and that within the broad Cr-band is up to $\sim$5 dB/m in the Cr, Er AGCYS fiber; hence, the fiber presents a case of heavily doping with both 'active' co-dopants.

3.2 Nonlinear Absorption

An important issue is the Cr, Er AGCYS fiber's optical nonlinearity that herein is addressed in terms of pump-power dependent absorption (loss). The featuring results are summarized in Fig. 5 for different excitation wavelengths: (a) falling into Er band absorption maximum, 976 nm (the 'resonant' case) and (b) off Er band while into Cr broad absorption band, 905/1064 nm) (the 'non-resonant' case). Note that in Fig. 5(a) we compare the effect of nonlinear (bleached)

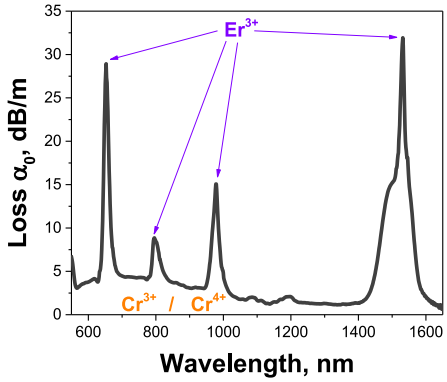

Fig. 4. Absorption spectrum of Cr, Er AGCYS fiber, where the spectral positions of Er^{3+} and Cr^{3+}/Cr^{4+} bands are highlighted.

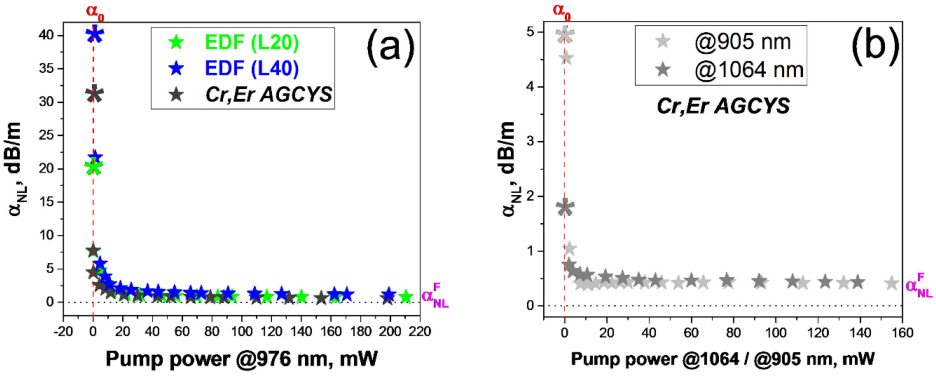

Fig. 5. (a) Dependences of nonlinear absorption (the bleaching effect) versus pump power @976 nm (into Er^{3+} absorption band), for Cr, Er AGCYS, EDF L20, and EDF L40 fibers. (b) Analogous dependences obtained for Cr, Er AGCYS fiber @905/1064 nm (both into Cr^{3+}/Cr^{4+} absorption band while off Er^{3+} absorption band). Asterisks designate the fibers' small-signal absorptions, obtained from the loss spectra measured with OSA (α_0); in turn, plateaus (α^F_{NL} – values) correspond to the unbleached absorptions of the fibers.

absorption in this fiber and those in two commercial Er-doped fibers: EDFs from Liekki/nLight Er20-4/125 (further – 'L20') and Er40-4/125 (further – 'L40'), having nominal absorptions at 1530 nm ~20 dB/m and ~40 dB/m, respectively [25]. As seen, in terms of Er content, the Cr, Er AGCYS fiber takes an intermediate position between EDFs L20 and L40.

In experiments, pump light from laser diodes (LDs) with operating wavelengths @976, 905, and 1064 nm was launched through splice to an active fiber sample with length L_f and its nonlinear transmission was measured, using a powermeter *(Thorlabs PM100D)*, as $T_{NL} = P_{out}/P_{in}$ (P_{in} is the launched pump power and P_{out} is its unabsorbed part), which was then re-calculated in nonlinear absorption (or loss) α_{NL} via relationship: $\alpha_{NL} = -\ln(T_{NL})/L_f$. Such dependences were obtained for all active fibers under study for the broad range of pump powers P_{in}; the results are presented in Fig. 5(a, b). Note that lengths L_f of fiber samples were chosen to be reciprocal of small-signal absorption α_0, thus ensuring nearly equal optical densities (OD $= \alpha_0 L_f$, the quantity characterizing attenuation in the samples).

As seen from Fig. 5(a), the dependences $\alpha_{NL}(P_{in})$ @976 nm (at resonant, viz. into Er band, excitation), for all active fibers examined, are easily bleachable and demonstrate similar behaviors: in spite of quite different linear absorptions (attributed by α_0-values; see the asterisks), all the dependences approach nearly the same plateaus (α^F_{NL}) at high pump powers; meanwhile α^F_{NL}

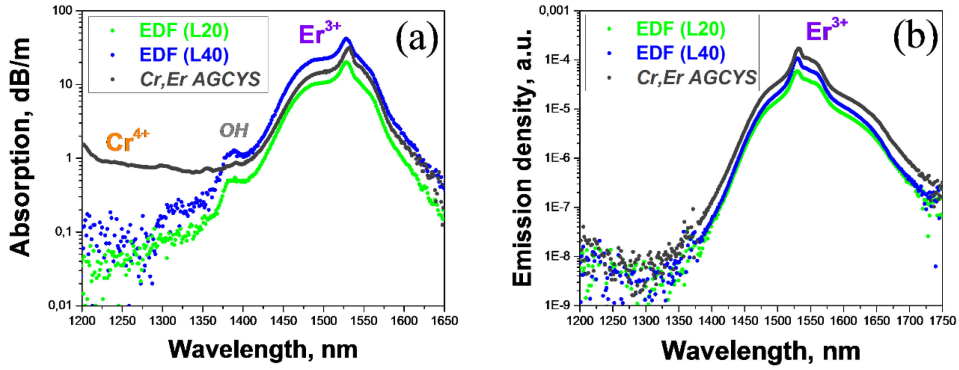

Fig. 6. Comparison of NIR (a) absorption and emission and (b) spectra of Cr, Er AGCYS fiber (∼30 dB/m) (black curves) with Cr-free EDFs (L20 and L40) with comparable (∼20 dB/m and ∼30 dB/m, respectively) extinctions in Er^{3+} peak @1530 nm (green and blue curves). The emission spectra were measured in frontal geometry at 976-nm pumping with the same power (∼110 mW), using the fibers' lengths providing the same OD of all three samples handled.

is minimal for the Cr, Er AGCYS fiber. Furthermore, as seen from Fig. 5(b), this fiber is easily bleachable at non-resonant (off Er band) excitation, too, thus revealing effective bleaching of the broad absorption band, inherent to co-doping with Cr. The residual (unbleached) losses α_{NL}^{F} may be of a varied origin: these may arise in both Er and Cr subsystems via excited-state absorption and/or up-conversion (UC) due to the ions clustering [25]. In any case, these effects are not significant in all fibers examined, including the Cr, Er AGCYS fiber, at any kind of excitation. The absorption contrasts (α_{NL}^{F}/α_0) for the Cr, Er AGCYS fiber are found to be ∼0.03 @976 nm (Er^{3+} band) and ∼0.08 @905/1064 nm (Cr^{3+}/Cr^{4+} band); the data are summarized in Table 1.

3.3 Emission Spectra and Lifetimes

In Fig. 6(a), we repeat the absorption spectrum of the Cr, Er AGCYS fiber in NIR (1200–1650 nm) and compare it with the analogous spectra of two commercial heavily-doped with Er fibers: EDFs L20 and L40. In addition to the features stemming from the presence of Cr ions in the Cr, Er AGCYS fiber, it demonstrates lower loss @1380 nm (a signature of hydroxyl OH-groups) than in the commercial (L20/L40) EDFs, which is an advantage for applications.

Accordingly, in Fig. 6(b), we demonstrate the emission spectra (in NIR: 1200–1750 nm) of these three fibers at 976-nm excitation of the same power (∼110 mW), collected from tips of fiber samples with lengths providing nearly the same OD. Experimentally, fiber samples were in-core pumped through splices in the simplest forward geometry by a commercial 976-nm LD (*JDSU*) with single-mode output fiber. The same OD of the Cr, Er AGCYS, L20, and L40 fibers and the same geometry of pump-light launching and emission detection ensured worthiness of comparison of the plotted emission spectra for these three fibers. Thus, from Fig. 6(b), we conclude a higher emissive potential of the Cr, Er AGCYS fiber in NIR (1200–1750 nm) as compared to commercial L20/L40 (Cr-free) EDFs. Seemingly, this relates to co-doping of the former fiber with Cr^{3+}/Cr^{4+} ions and lower NIR fluorescence quenching due to reduced content of OH-groups (refer to Fig. 6(a)).

We also examined character of UC emission in these three fibers, using the same pump arrangement at 976-nm excitation. As seen from the photos of the fibers' lateral visible (mostly green) UC emission, obtained at equal excitation conditions (Fig. 7), its intensity in the Cr, Er fiber (Er^{3+} absorption, ∼30 dB/m) does not exceed that in EDF L20 (Er^{3+} absorption, ∼20 dB/m) while is much weaker than that in EDF L40 (Er^{3+} absorption, ∼40 dB/m). This may point on a weaker effect of Er ions clustering in the Cr, Er fiber than in the commercial EDFs, which probably stems from a more homogeneous distribution of active ions in the former fiber given its co-doping with Y; however,

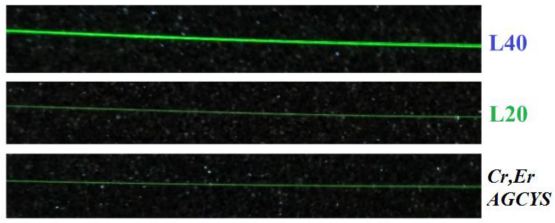

Fig. 7. Snapshots of lateral UC emission in VIS, for (a) EDF L40, (b) EDF L20, and (c) Cr, Er AGCYS fiber (excitation @976 nm, pump power ~250 mW), recorded for the fibers' segments (~10 cm in length), adjacent to splicing points with 976-nm LD output fiber.

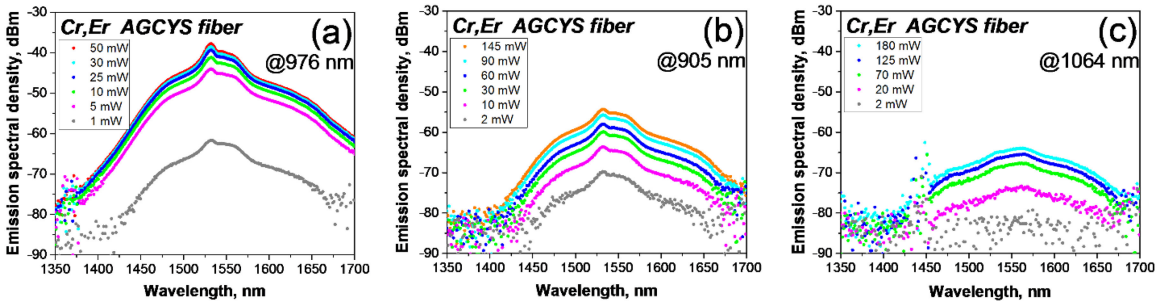

Fig. 8. NIR frontal emission spectra (Er^{3+} band) of Cr, Er AGCYS fiber ($L_f = 17$ cm) at different excitation wavelengths: (a) @976 nm, (b) @905 nm, and (c) @1064 nm, at different pump powers.

partial reabsorption of UC emission by Cr ions, having notable absorption in the visible (Fig. 4), cannot be dismissed as another mechanism behinds the observation.

The emission spectra of the Cr, Er AGCYS fiber within the Er^{3+} band (1350–1700 nm) are shown in Fig. 8 both for (a) resonant (into Er^{3+} band, @976 nm) and (b, c) non-resonant (off Er^{3+} band while into Cr^{3+}/Cr^{4+} band, @905/1064 nm) excitations.

Experimentally, the fiber samples were in each case in-core pumped by fiber-coupled commercial LDs through splices and the emission spectra were detected at their outputs. For worthiness of comparison, the results are exemplified for the same length of Cr, Er AGCYS fiber ($L_f = 17$ cm).

Note that the presence of Er^{3+} related NIR emission @905/1064 nm excitations (b, c) evidences an effective energy transfer from Cr^{3+}/Cr^{4+} subsystem to Er^{3+} one, however much less pronounced in the latter case. The revealed effect of indirect excitation of Er^{3+} fluorescence in mixed Cr, Er system is reported for the first time to the best of our knowledge.

Regarding the resonant excitation @976 nm, note that Er^{3+} emission has in this case 'common' character, where its maximum shifts to the Stokes side with increasing length of the Cr, Er AGCYS fiber; see Fig. 9(a). Also note that, due to a high amplifying potential of the Cr, Er AGCYS fiber (see Section 3.4), amplified spontaneous emission (ASE) easily transforms to spurious lasing within the Er^{3+} band (due to Fresnel reflection on the fiber's cleaved ends) at increasing pump power for L_f varied between ~70 and ~380 cm; see the examples of such scenarios in Fig. 9(b, c). Expectedly, for shorter pieces of the fiber, spurious lasing is established near the Er^{3+} fluorescence maximum (~1530 nm, (b)) whereas at longer pieces of the fiber its central wavelength shifts to the Stokes side (up to ~1560 nm, (c)) where optimal conditions are created for the maximal inversion in the Er^{3+} ions system.

Note that the type of the Cr, Er AGCYS fiber's emission at non-resonant (off Er^{3+} band while within Cr^{3+}/Cr^{4+} band) excitation is different: in Fig. 10 we present the results of the experiment on pumping the fiber @905 nm.

In this case, as seen from Fig. 10, in addition to the NIR emissions characteristic to Cr^{3+}/Cr^{4+} ions (barely structured within the 1.0–1.5 μm range), there also appears powerful fluorescence

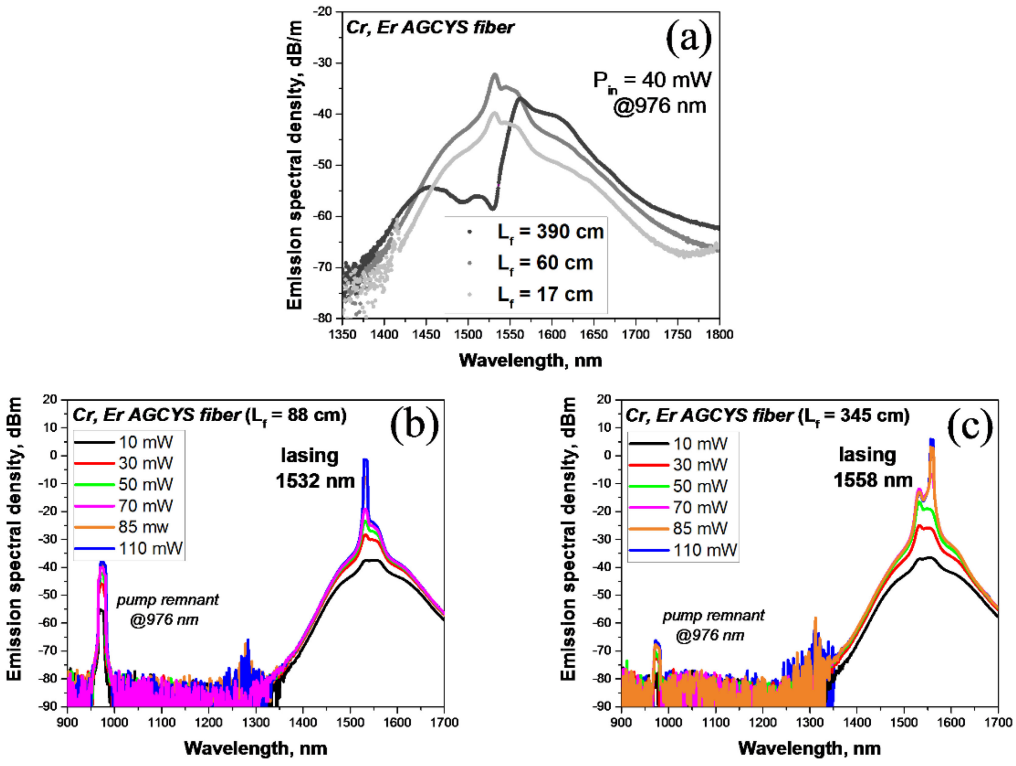

Fig. 9. (a) Frontal emission spectra of Cr, Er AGCYS fiber at different lengths of samples and the same pump power @976 nm (below threshold of spurious lasing). (b, c) Two examples of spectral response of the fiber (for shorter and longer lengths), viz. spurious lasing at (b) ~1532 nm (peak of emission band of Er^{3+} ions) ($L_f = 88$ cm) and (c) at ~1558 nm (corresponding to maximal spectral inversion in Er^{3+} subsystem) ($L_f = 345$ cm). The data are collected for growing pump power @976 nm.

inherent to Er^{3+} ions due to already mentioned energy transfer from Cr^{3+}/Cr^{4+} subsystem to Er^{3+} subsystem (refer to Fig. 8(b)).

In analogy to the case of resonant excitation @976 nm (see Fig. 9(a)), maximum of Er^{3+} fluorescence shifts to longer wavelengths with increasing fiber length L_f, as seen from Fig. 10(a), where are provided the NIR emission spectra for maximal available pump power @905 nm. For the sake of completeness, we show in Fig. 10(b, c) such spectra in function of pump power @905 nm for $L_f = 58$ and 370 cm, respectively.

On the contrary to resonant excitation (compare with Fig. 9(b, c)), no spurious lasing in Er^{3+} subsystem arises at this kind of excitation because in this case energy transfer from Cr^{3+}/Cr^{4+} to Er^{3+} is not effective to establish a high gain and threshold conditions for lasing.

In Fig. 11(a, b), to complete the pattern of emissive potential of the Cr, Er AGCYS fiber, we present the data of NIR (>1 μm) fluorescence decay measurements, acquired at both kinds – resonant (@976 nm) and non-resonant (@905 nm) – of excitation; the results are summarized in Table 1.

The data were collected in backward geometry, using a specially handpicked wavelength-division multiplexor (WDM) to separate pump light and detected NIR emission. The NIR (up to ~1.6 μm) fluorescence signals from fiber samples were collected after fast switching pump light off. To further mitigate pump background in the measured signal, a long-pass 1000-nm optical filter (*Thorlabs FEL1000*) was placed between a fiber sample and a Ge-based photo-detector (*Newport 2033*, 200-kHz bandwidth). To avoid any effect of reabsorption, relatively short fiber samples were employed: $L_f = 7$ and 11 cm @976 and @905 nm, respectively. The time resolution of the measurements was ~8 μs.

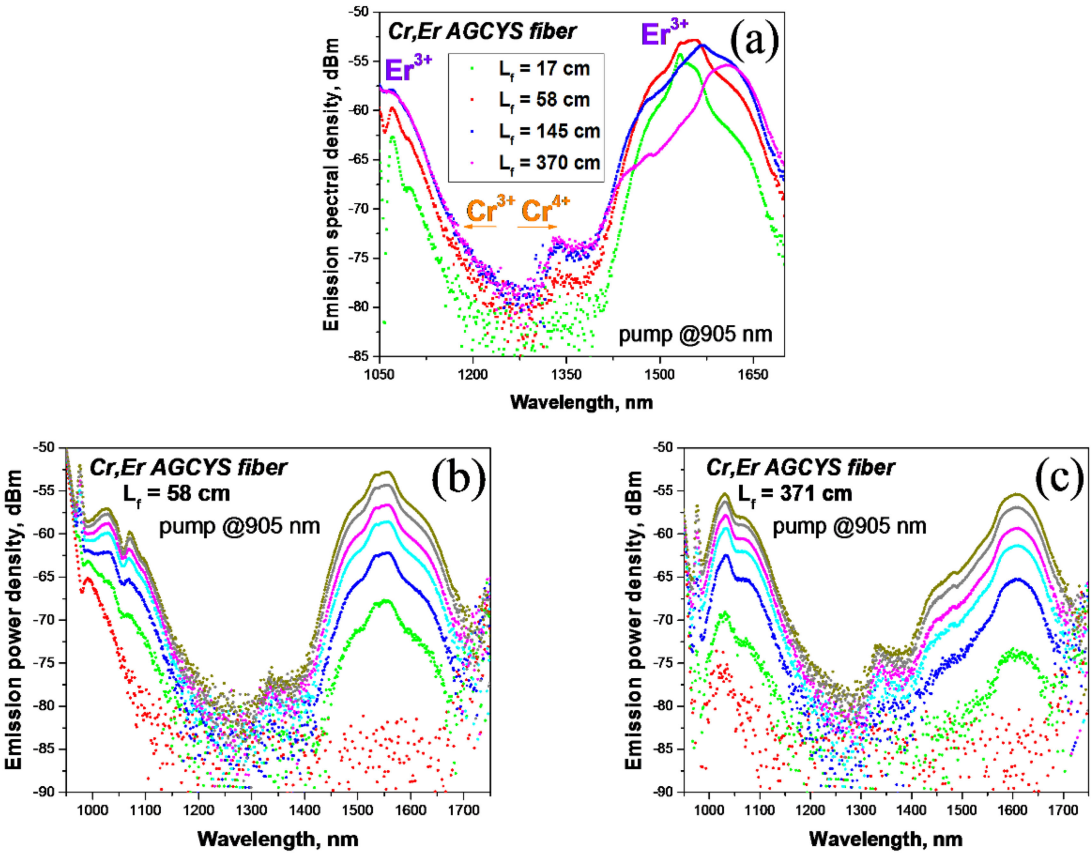

Fig. 10. (a) Frontal emission spectra of Cr, Er AGCYS fiber @905-nm excitation (140 mW) (into Cr^{3+}/Cr^{4+} absorption band while off Er^{3+} absorption band) for different fiber lengths L_f; spectral positions of NIR emissions, adherent to Cr^{3+}/Cr^{4+} and Er^{3+} subsystems, are highlighted. (b, c) Frontal emission spectra of the fiber @905-nm excitation at increasing pump power, exemplified by 1, 4, 16, 35, 57, 98, and 140 mW, obtained for different lengths L_f: (b) 58 cm and (c) 371 cm.

As one can reveal from Fig. 11, the decay kinetics are always composed of two exponents, highlighted by the arrows, with decay times of ~9.8 ms and ~40 μs, respectively; the contribution of the latter produces a slight deformation in the overall kinetics in Fig. 11(a) and looks as abrupt drop in the decay kinetics in Fig. 11(b), both details arisen just after pump-light switching off. These two exponents can be ascribed to the contributions of Er^{3+} and Cr^{3+}/Cr^{4+} ions, respectively. Note that for both excitation wavelengths, the decay times were found to be virtually independent of pump power, at least for their low levels.

3.4 Gain

We also made insight to the spectral features of amplifying potential (gain) of the Cr, Er AGCYS fiber. First, we compared net gain in this fiber and in commercial Cr-free EDFs L20 and L40 at the resonant (into Er band) 976-nm excitation and then examined what happens with it at the non-resonant (off Er band while into Cr-band) 905/1064-nm excitations. All experiments were proceeded in equal experimental conditions, applying the following procedure. An active fiber sample was pumped from its one side by a LD (@976, @905, or @1064 nm) through a WDM and a small signal to be amplified was delivered from the WL source from its opposite side. By means of measuring the fiber's emission spectra at WL switched on and off, then measuring its attenuation spectrum without pumping (while with WL switched on), and posterior data processing, net gain spectra (in dB/m)

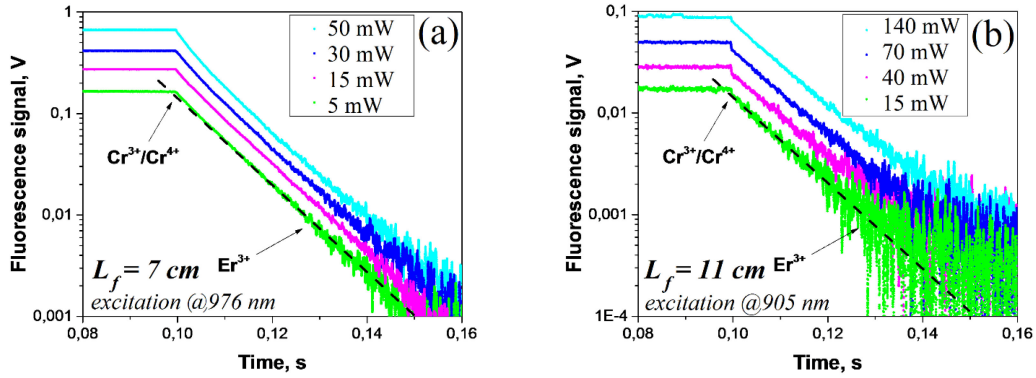

Fig. 11. NIR fluorescence decay kinetics in Cr, Er AGCYS fiber at (a) 976-nm and (b) 905-nm excitations at different pump powers, detected in backward geometry using short fiber samples.

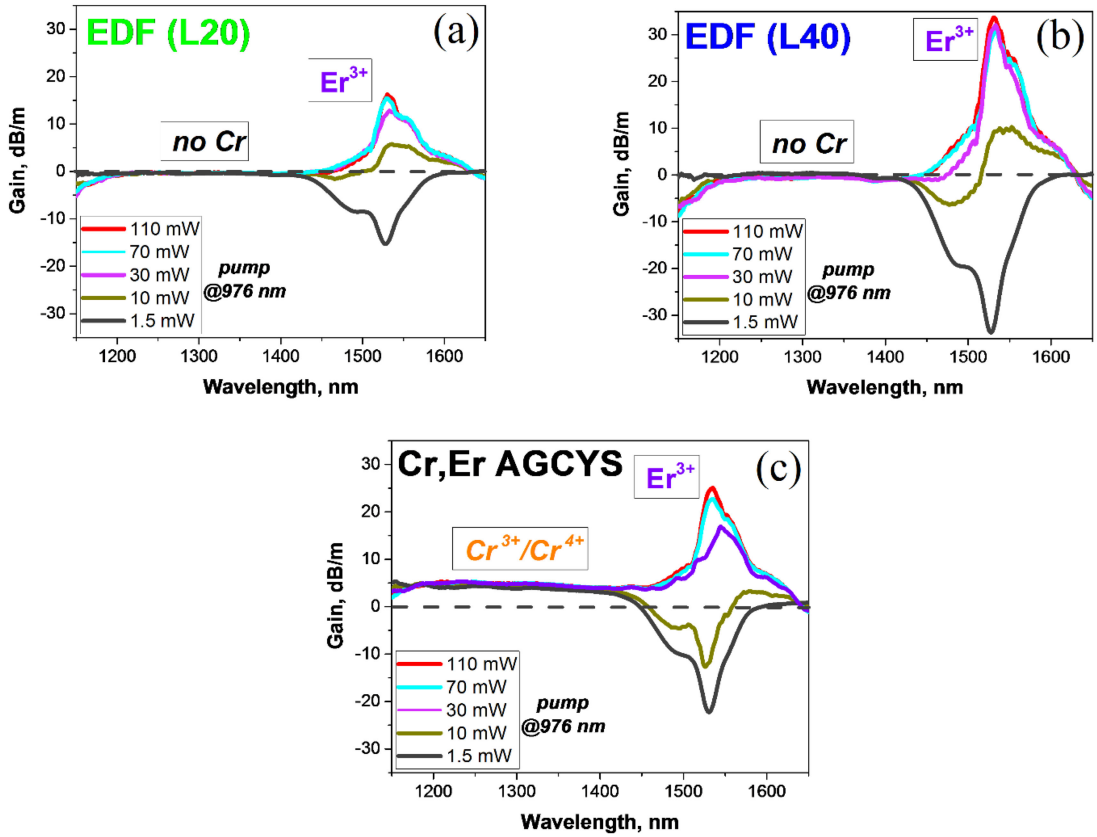

Fig. 12. Spectral dependences of net gain in (a) EDF L20, (b) EDF L40, and (c) Cr, Er AGCYS fiber in NIR (1150–1650 nm), measured at excitation by LD with operating wavelength 976 nm; launched pump powers are specified in insets.

were found. In the experiments, we used the same WDM as in the lifetime measurements, reported above.

The results for 976-nm pumping at different pump power are shown in Fig. 12 where are compared the data obtained for commercial L20/L40 EDFs (a, b) and those for the Cr, Er AGCYS fiber (c).

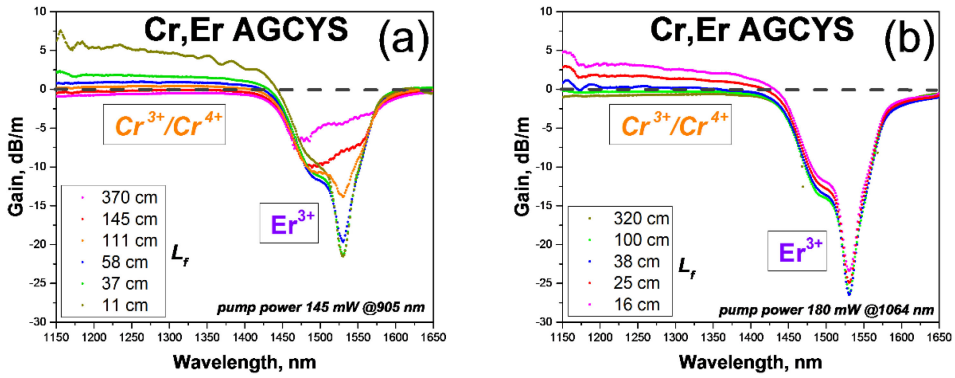

Fig. 13. Spectral dependences of net gain in Cr, Er AGCYS fiber in NIR (1150–1650 nm), measured at excitation by LDs with operating wavelengths (a) 905 nm and (b) 1064 nm; launched pump powers at these wavelengths and lengths L_f of the fiber samples under study are specified in insets.

One can see from Fig. 12 the two main advantages the new fiber provides. First, as seen from Fig. 12(c), maximal gain (@1530 nm) in the Cr, Er AGCYS fiber at full Er^{3+} absorption saturation (>50 mW) reaches g_0 ~28 dB/m, i.e., the value only a bit lower than its small-signal absorption (α_0 ~32 dB/m); importantly, the ratio g_0/α_0 approaches ~0.87. This reveals a quite big amplifying potential of the fiber, even better than provide the commercial EDFs L20/L40 (α_0 ~21/40 dB/m; g_0 ~17/32 dB/m; g_0/α_0 ~0.82/0.81); see Fig. 12(a, b). Second, in difference to the commercial EDFs that do not amplify at 1.15–45 μm (given the absence of Cr ions), the Cr, Er AGCYS fiber possesses broadband plain positive net gain in this spectral domain (g_0 ~3–4 dB/m), apparently because of co-doping with Cr^{3+}/Cr^{4+} ions. Seemingly, this effect is not only produced by the direct excitation of Cr^{3+}/Cr^{4+} ions by pumping @976 nm but, also, by means of energy transfer from excited states of Er^{3+} ions.

Furthermore, analogous measurements of spectrally-dependent gain in the Cr, Er AGCYS fiber were done using LDs @905/1064 nm as pump sources; see Fig. 13(a) and (b), respectively, viz. via excitation off Er^{3+} absorption band while into Cr^{3+}/Cr^{4+} one. We limit ourselves here by snapshotting the results for maximal available pump powers (145 mW and 180 mW, respectively). The plotted spectra were obtained for different lengths of the Cr, Er AGCYS fiber to shed more light on the physics of energy transfer between Er^{3+} and Cr^{3+}/Cr^{4+} subsystems at these kinds of non-resonant excitation.

As seen from Fig. 13, in both cases, there is positive, more-or-less plain gain within the range ~1150 to ~1400 nm, inherent to Cr ions in the Cr, Er AGCYS fiber, which are effectively inverted under the action of pump light. However, at increasing length of the fiber, gain within this spectral range gets worsen, the effect explained not only by common effect of depletion of pump light along fiber length but, also, by leakage of excitation, accumulated in Cr subsystem, to Er subsystem, seen as bleaching of resonant absorption within Er^{3+} band.

4. Conclusions

In this work, we report fabrication and complex analysis of the basic material and optical properties of new Chromium, Erbium (Cr, Er) co-doped alumina-germania-calcia-yttria-silica (AGCYS) fiber. To the best of our knowledge, it is the first successful realization of Cr/Er co-doping in a silica-based fiber as no earlier reports on the matter are found in the literature. Furthermore, the fabricated fiber is straightforwardly compared with commercial Er-doped fibers (EDFs) of 'L20' (Er20-4/125) and 'L40' (Er40-4/125) types. As shown, the novel Cr, Er AGCYS fiber demonstrates in the NIR region all optical properties inherent to doping with Er^{3+} ions, well-known for EDFs, as well as the advantageous features stemming from co-doping with Cr^{3+}/Cr^{4+} ions. This concerns a set of characteristics impactful for NIR (>1 μm) applications, viz. absorption and fluorescence spectra,

fluorescence decay, resonant-absorption bleaching, and gain spectra. Importantly, we measured the latter characteristics at different wavelengths (976, 905, and 1064 nm), falling into resonant-absorption bands of Er^{3+} and Cr^{3+}/Cr^{4+} ions, which allows to uncover the details of direct excitation of these two subsystems and, also, energy transfer between them. Among the found perspective features of the Cr, Er AGCYS fiber, note its high quality in terms of the ratio of bleached-to-residual resonant absorption and the ratio of net gain to small-signal absorption (at 976-nm pumping), both impactful for NIR applications at in-core diode pumping. Also, note the reduced up-conversion in the fiber and relatively long NIR fluorescence lifetimes, inherent to the presence of both Er^{3+} and Cr^{3+}/Cr^{4+} ions. The latter advantage can be assigned to almost ideal core-glass structure of the fiber, facilitating – because of the presence of Al/Y precursors – the homogeneous dispersion of both 'active' co-dopants (Cr/Er) in the core-glass and, eventually, diminished clustering effects.

Acknowledgment

The authors would like to thank the Director of CSIR-CGCRI for his continuous support and encouragement. Mr. D. Dutta would like to thank the Department of Science and Technology, Government of India, for providing the fellowship. The authors are also grateful to Dr. A. Halder (Kolkata, India) for making modeling of modal guidance of the fabricated fiber and to Dr. Y. Barmenkov (Leon, Mexico) for fruitful discussions.

References

[1] V. V. Dvoyrin, V. M. Mashinsky, E. M. Dianov, A. A. Umnikov, M. V. Yashkov, and A. N. Guranov, "Absorption, fluorescence and optical amplification in MCVD bismuth-doped silica glass optical fibres," in *Proc. 31st Eur. Conf. Opt. Commun.*, 2005, vol. 4, pp. 949–950.
[2] E. M. Dianov, "Bismuth-doped optical fibres: A new breakthrough in near-IR lasing media," *Quantum Electron.*, vol. 42, pp. 754–761, 2012.
[3] E. M. Dianov, "Amplification in extended transmission bands using bismuth-doped optical fibers," *J. Lightw. Technol.*, vol. 31, no. 4, pp. 681–688, Feb. 2013.
[4] V. Felice, B. Dussardier, J. K. Jones, G. Monnom, and D. B. Ostrowsky, "Cr^{4+}-doped silica optical fibres: Absorption and fluorescence properties," *Eur. Phys. J.—Appl. Phys.*, vol. 11, pp. 107–110, 2000.
[5] S.-M. Yeh *et al.*, "Broadband chromium-doped fiber amplifiers for next generation optical communication systems," *J. Lightw. Technol.*, vol. 30, no. 6, pp. 921–927, Mar. 2012.
[6] S. Unger, A. Schwuchow, J. Dellith, and J. Kirchhof, "Codoped materials for high power fiber lasers: Diffusion behavior and optical properties," in *Proc. SPIE*, 2007, Art. no. 646913.
[7] Y. Luo, J. Wen, J. Zhang, J. Canning, and G.-D. Peng, "Bismuth and erbium codoped optical fiber with ultrabroadband luminescence across O-, E-, S-, C-, and L-bands," *Opt. Lett.*, vol. 37, 2012, Art. no. 34473449.
[8] J. Zhang, Z. M. Sathi, Y. Luo, J. Canning, and G.-D. Peng, "Toward an ultra-broadband emission source based on the bismuth and erbium co-doped optical fiber and a single 830 nm laser diode pump," *Opt. Exp.*, vol. 21, pp. 7786–7792, 2013.
[9] Z. M. Sathi, J. Zhang, Y. Luo, J. Canning, and G. D. Peng, "Improving broadband emission within Bi/Er doped silicate fibres with Yb co-doping," *Opt. Mater. Exp.*, vol. 5, pp. 2096–2105, 2015.
[10] B. Yan, Y. Luo, A. Zareanborji, G. Xiao, G.-D. Peng, and J. Wen, "Performance comparison of bismuth/erbium co-doped optical fibre by 830 nm and 980 nm pumping," *J. Opt.*, vol. 18, 2016, Art. no. 105705.
[11] Y. Luo *et al.*, "Systematical study of up-conversion and near infrared emission of Bi/Er co-doped optical fibre pumped at 830 nm," *Optik*, vol. 133, pp. 132–139, 2017.
[12] Y. Luo, B. Yan, J. Zhang, J. Wen, J. He, and G.-D. Peng, "Development of Bi/Er co-doped optical fibers for ultrabroadband photonic applications," *Frontiers Optoelectron.*, vol. 11, pp. 37–52, 2018.
[13] D. Chen, H. Fu, W. Liu, Y. Wei, and S. He, "Dual-wavelength single-longitudinal-mode erbium-doped fibre laser based on fibre Bragg grating pair and its application in microwave signal generation," *Electron. Lett.*, vol. 44, pp. 458–460, 2008.
[14] Y. Yao, X. Chen, Y. Dai, and S. Xie, "Dual-wavelength erbium-doped fiber laser with a simple linear cavity and its application in microwave generation," *IEEE Photon. Technol. Lett.*, vol. 18, no. 1, pp. 187–189, Jan. 2006.
[15] H. Ahmad, M. R. K. Soltanian, C. H. Pua, M. Alimadad, and S. W. Harun, "Photonic crystal fiber based dual-wavelength Q-switched fiber laser using graphene oxide as a saturable absorber," *Appl. Opt.*, vol. 53, pp. 3581–3586, 2014.
[16] M. R. K. Soltanian, I. S. Amiri, W. Y. Chong, S. E. Alavi, and H. Ahmad, "Stable dual-wavelength coherent source with tunable wavelength spacing generated by spectral slicing a mode-locked laser using microring resonator," *IEEE Photon. J.*, vol. 7, no. 6, Dec. 2015, Art. no. 1504311.
[17] M. R. K. Soltanian, I. S. Amiri, S. E. Alavi, and H. Ahmad, "Dual-wavelength erbium-doped fiber laser to generate terahertz radiation using photonic crystal fiber," *J. Lightw. Technol.*, vol. 33, no. 24, pp. 5138–5146, Dec. 2015.

[18] M. Hatipoğlu and Ç. Barutcigil, "Effects of erbium-and chromium-doped yttrium scandium gallium garnet and diode lasers on the surfaces of restorative dental materials: A scanning electron microscope study," *Nigerian J. Clin. Pract.*, vol. 18, pp. 213–220, 2015.
[19] D. Dutta, A. Dhar, A. V. Kir'yanov, S. Das, S. Bysakh, and M. C. Paul, "Fabrication and characterization of chromium-doped nanophase separated yttria–alumina–silica glass-based optical fibers," *Physica Status Solidi A*, vol. 212, pp. 1836–1844, 2015.
[20] A. V. Kir'yanov *et al.*, "Basic and peculiar properties of chromium–magnesium co-doped YAS-based optical fiber," *IEEE J. Quantum Electron.*, vol. 52, no. 7, pp. 1–12, Jul. 2016.
[21] S. R. Nagel, J. B. MacChesney, and K. L. Walker, "An overview of the modified chemical vapor deposition (MCVD) process and performance," *IEEE Trans. Microw. Theory Techn.*, vol. MTT-30, no. 4, pp. 459–476, Apr. 1982.
[22] S. Addanki, I. S. Amiri, and P. Yupapin, "Review of optical fibers—Introduction and applications in fiber lasers," *Res. Phys.*, vol. 10, pp. 743–750, 2018.
[23] J. E. Townsend, S. B. Poole, and D. N. Payne, "Solution-doping technique for fabrication of rare-earth doped optical fibres," *Electron. Lett.*, vol. 23, pp. 329–331, 1987.
[24] J. Kobelke *et al.*, "Diffusion and interface effects during preparation of all-solid microstructured fibers," *Materials*, vol. 7, pp. 6879–6892, 2014.
[25] A. V. Kir'yanov, Y. O. Barmenkov, G. E. Sandoval-Romero, and L. Escalante-Zarate, "Er^{3+} concentration effects in commercial erbium-doped silica fibers fabricated through the MCVD and DND technologies," *IEEE J. Quantum Electron.*, vol. 49, no. 6, pp. 511–521, Jun. 2013.